https://doi.org/10.1130/G50673.1

Manuscript received 15 August 2022 Revised manuscript received 12 October 2022 Manuscript accepted 28 October 2022

Published online 20 January 2023

© 2023 Geological Society of America. For permission to copy, contact editing@geosociety.org

A power-based abrasion law for use in landscape evolution models

D.D. Hansen¹, J.P. Brooks¹, L.K. Zoet^{1,2}, N.T. Stevens¹, L. Smith¹, C.E. Bate² and B.J. Jahnke²
¹Department of Geoscience, University of Wisconsin–Madison, 1215 W. Dayton Street, Madison, Wisconsin 53706, USA
²Department of Geological Engineering, University of Wisconsin–Madison, 1415 Engineering Drive, Madison, Wisconsin 53706, USA

ABSTRACT

Subglacial abrasion drives erosion for many glaciers, inundating forefields and proglacial marine environments with glaciogenic sediments. Theoretical treatments of this process suggest that bedrock abrasion rates scale linearly with the energy expended through rock-on-rock friction during slip, but this assumption lacks an empirical basis for general implementation. To test this approach, we simulated abrasion by sliding debris-laden ice over rock beds under subglacial conditions in a cryo-ring shear and a direct shear device. Miniscule volumes of erosion that occurred during each run were mapped with a white-light profilometer, and we measured the rock mechanical properties needed to constrain the energy expended through abrasion. We find that abraded volume per unit area increases linearly with average shear force at the bed and that abrasion rates increase linearly with basal power for plane beds. Lastly, only a small percentage (1%) of the energy partitioned to basal slip is dissipated by abrasion. These results confirm the basal-power abrasion rule is viable to implement in landscape evolution models.

INTRODUCTION

Glaciers and ice sheets erode bedrock at faster rates than most fluvial and aeolian systems (Hallet et al., 1996). Throughout geologic time, they have sculpted high-latitude landscapes, exposing their iconic bedforms as they recede (Benn and Evans, 2010). This persistent denudation modulates Earth's climate through a series of feedbacks linking climate, tectonics, and erosion (Molnar and England, 1990), and drag imparted by eroded clasts regulates ice flux to the oceans (Alley et al., 2019). Nevertheless, simulating glacial erosion using physically motivated erosion laws in landscape evolution models (LEMs) is challenging due to the difficulty of constraining its phenomenological controls.

Fundamentally, glacial erosion arises from the gravitationally driven motion of ice, set by the distribution of ice mass and underlying catchment topography (Andrews, 1972). As glaciers move from high to low elevations, stored potential energy dissipates at first order through the internal deformation of ice (Nye, 1957), the melting of snow and ice (Nye, 1976), and basal slip (Weertman, 1957). Energy partitioned to basal slip facilitates the mechanical wear of bedrock through abrasion and quarrying (Drewry, 1986). Thus, the total power available to erode

the substrate is some fraction of the work done by ice slipping over rock per unit area (W_b) per unit time, sometimes termed "basal power":

$$\dot{W}_{\rm b} \equiv \frac{dW_{\rm b}}{dt} = u_{\rm s} \tau_{\rm b},\tag{1}$$

where u_s is slip speed of ice, t is time, and τ_b is basal shear stress (Hallet, 2011). Expressed differently, energy dissipated through abrasion and quarrying limits the finite amount of energy available for the physical processes that facilitate slip (regelation and viscous deformation), although the extent of energy dissipation is largely unknown.

Given that the physics governing rock-on-rock friction at the ice-bed interface are identical to those of a typical fault system (Zoet et al., 2013), one might expect these energy expenditures to fall within the same order of magnitude. Previous estimates suggest that $\sim 30\%$ –40% of \dot{W}_b is dissipated through abrasion (Metcalf, 1979), which would have considerable ramifications for slip dynamics. However, these studies are based on field data with large uncertainties (Metcalf, 1979), and their results seemingly contradict modern observations of energy partitioning in active faults, which commonly report

 \sim 1% (Fulton and Rathbun, 2011, and references therein).

Currently, the relationship between abrasion rates and basal power is tenuous and therefore so is the proper form of the abrasion law. A link between these two variables is implicitly reflected in Hallet's (1979) widely used model for glacial abrasion. He proposed a simple wear law of the form

$$\dot{A} = \alpha C F_{\rm n}^{\ l} u_{\rm p},\tag{2}$$

where A is the abrasion rate, α represents the erodibility of the rock and relates to clast angularity and the hardness contrast with the bed, C is the areal concentration of debris, l is an empirical constant typically assumed to be unity, u_p is particle velocity, and F_p is the average bednormal contact force between clasts and the bed. Assuming Coulomb friction, the drag, τ_r , arising from subglacial rock friction equals μF_n where μ is the coefficient of friction. This implies that A scales with the work expended through rock frictional energy per unit time, $\mu F_n u_s$ (Hallet, 2011). From this follows a simple abrasion rule that can be implemented in LEMs and is analogous to the stream-power rules commonly used to model fluvial erosion (Whipple and Tucker, 1999):

$$\dot{A} = KC \tau_{\rm r} u_{\rm s},\tag{3}$$

where K is an erodibility constant. A benefit of this basal-power approach is that it does not assume specific controls on F_n , which are commonly uncertain and can deviate from Hallet's (1979) conceptual model (Hansen and Zoet, 2019; Thompson et al., 2020). Linearity between \dot{W}_b and \dot{A} , as implemented in LEMs (Hallet, 2011; Ugelvig and Egholm, 2018), assumes a linear relationship between τ_r and τ_b . Paired with a quarrying rule in LEM runs, Equation 3 has produced realistic and spatially heterogeneous erosion rates characteristic of natural systems

CITATION: Hansen, D.D., et al., 2023, A power-based abrasion law for use in landscape evolution models: Geology, v. XX, p. G50673.1

, https://doi.org/10.1130/

(Ugelvig and Egholm, 2018), but the empirical basis for its use remains unverified. This uncertainty stems from the difficulty of measuring \dot{A} in the field and of measuring abrasion in the laboratory due to the complexity of replicating in situ conditions and the miniscule amounts of erosion that occur over the short duration (days to weeks) of these experiments.

In this study, we created the most realistic laboratory simulations of glacial abrasion to date and used a high-precision profilometer to measure erosion that occurred during basal slip. With these data, we examine the relationships between abrasion, the work done during slip, and the energy dissipated through striating rock to assess the viability of the basal-power approach for modeling abrasion.

METHODS

To quantify the relationship between rock frictional energy and \dot{A} , we used a cryogenic ring shear (RS) device (Hansen and Zoet, 2022) and a direct shear (DS) device with a custom sample chamber to slide temperate ice laden with granitoid clasts over beds of marble and limestone, following published methods (see sections S1 and S2 in the Supplemental Material¹). We prescribed a range of realistic sliding velocities, normal stresses, debris concentrations, and basal melt rates (Table 1)-known controls on debrisbed friction and A (Thompson et al., 2020, and references therein). For the limestone-bed experiments, 12 very angular, granitic rock fragments with high sphericity were encased in ice in contact with the bed. Both the angularity of these clasts and their hardness contrast relative to the soft limestone are greater than in most glacier settings and therefore serve as an end-member case. For the marble runs, we sourced subangular to subrounded granitic clasts from subgla-

'Supplemental Material. A detailed description of the experimental methodology and the CCNBD and UTC results. Please visit https://doi.org/10.1130/GEOL.S.21824817 to access the supplemental material, and contact editing@geosociety.org with any questions.

cial till. We intentionally selected hard clasts to minimize comminution of the abraders and isolate the effects of abrasion. Striations were scanned with a white-light interferometer (3 μ m lateral accuracy at 17 nm height repeatability) to create digital elevation models (DEMs) of the abraded surface. From these DEMs, we calculated eroded volume, V, by fitting a plane to the surface and quantifying the volume enclosed between the abraded surface and this plane (our workflow is described in section S3 of the Supplemental Material).

The energy consumed through abrasion is defined as

$$E_{\rm a} = \gamma \Delta S,$$
 (4)

where γ is the specific surface fracture energy of the rock (energy required to break bonds and thus create new surface area) and ΔS is the difference between the initial surface area of the bed and the surface area post-shear (Fulton and Rathbun, 2011). We derived γ for both lithologies using measurements of fracture toughness obtained with cracked-chevron, notched Brazilian disc (CCNBD) tests and estimates for Young's modulus and Poisson's ratio obtained from uniaxial unconfined compression tests (UCTs) (see section S5 of the Supplemental Material for derivation, methods, and CCNBD and UCT results).

The change in surface area following abrasion is defined as

$$\Delta S = S_{\text{surf}} - S_{\text{init}} + S_{\text{p}}, \tag{5}$$

where S_{surf} is the surface area of the void contained within the striation, S_{init} is the initial surface area, and S_{p} is the surface area of the gouge particles. S_{p} is defined as

$$S_{\rm p} = R \sum_{i} \frac{6}{d_{\rm i}} \partial V_{\rm i} V, \tag{6}$$

where d and ∂V are the grain diameter and fractional volume, respectively, for a given size

TABLE 1. RUN PARAMETERS AND RESULTS

Experiment	Bed type	$a_{ m bed}$ (cm²)	$_{(kPa)}^{\sigma_{n}}$	(kPa)	u _s (m/yr)	$u_{\rm v}$ (mm/yr)	<i>Disp</i> (cm)	n _{clast}	n _{stria}	V (mm³)
RS1	М	2513.3	301	1.7	37.5	560	81.04	311	159	78.9
RS2	M	2513.3	302	4.2	37.5	780	71.26	311	291	178.7
DS1	М	100	200	24.4	200	1460	0.99	50	77	2.45
DS2	M	100	200	14.7	200	2086	0.87	50	50	1.65
DS3	M	100	200	74.1	200	2094	0.12	100	114	5.85
DS4	M	100	200	74.6	200	1600	0.92	100	150	4.47
DS5	M	100	200	53.7	200	1749	0.11	200	94	2.85
DS6	LS	100	294	13.4	526	944	0.995	12	17	14.6
DS7	LS	100	294	45.6	526	750	0.880	12	12	12.2
DS8	LS	100	294	93.5	526	50	0.972	12	17	3.93
DS9	LS	100	588	138.6	526	1370	0.943	12	15	21.9
DS10	LS	100	588	83.8	526	1210	1.102	12	14	37.8
DS11	LS	100	588	68.1	526	1270	0.926	12	19	25.7
DS12	LS	100	588	64.1	526	795	0.878	12	16	19.2
DS13	LS	100	294	76.0	526	584	0.953	12	12	14.9
DS14	LS	100	294	82.6	526	115	0.993	12	22	19.9

Notes: Experiment device: RS—ring shear; DS—direct shear. Bed type: M—marble; LS—limestone. a_{bed} bed area; σ_n —applied normal stress; τ_r —average shear stress; u_s —horizontal ice velocity; u_v —vertical ice velocity; Disp—displacement; n_{clast} —number of clasts; n_{stria} —number of striations; V—abraded volume.

fraction i, and R is a roughness factor correcting for the deviation of particle surface area from a sphere, which we set to be 4 ± 1 in line with previous work (Fulton and Rathbun, 2011). To constrain d_i , we slid clasts encased in epoxy slabs over both rock types and measured the grain-size distribution of the resulting gouge using laser diffraction analysis (see section S4 of the Supplemental Material). Mean grain diameters were $\sim\!90~\mu\mathrm{m}$ and $\sim\!95~\mu\mathrm{m}$ for limestone and marble, respectively, and S_p scales inversely with d. We do not include $S_{\mathrm{surf}} - S_{\mathrm{init}}$ in our calculations because it was more than two orders of magnitude smaller than S_p .

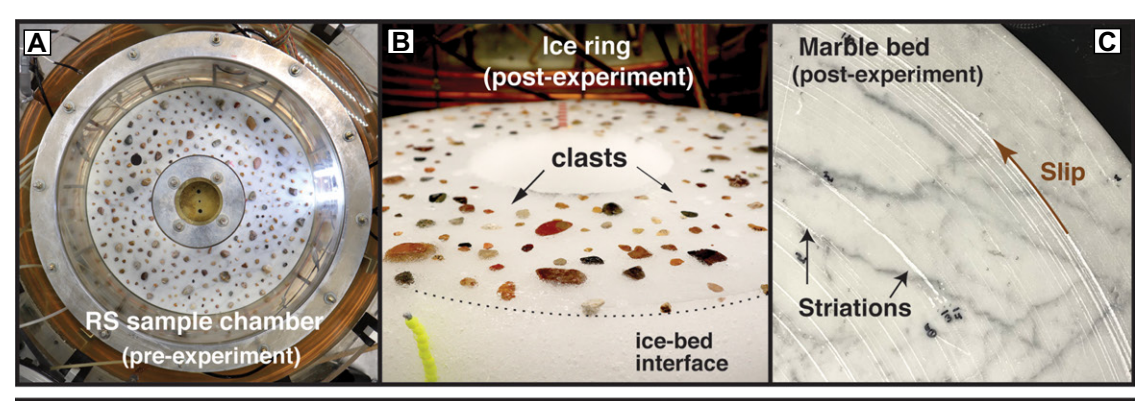
We employed a simple Monte Carlo Markov chain error propagation scheme to estimate the posterior distribution of E_a , using Equations 4–6 and Equations S1–S4 (see the Supplemental Material) for 20,000 randomly perturbed simulations (see section S6 of the Supplemental Material). We characterized linear trends by computing the regression coefficients and their associated standard error with an ordinary or weighted least-squares solution.

RESULTS

The striations produced in these experiments spanned the range of common forms in nature (Fig. 1) but commonly shallowed with increasing displacement in RS runs (Iverson, 1991). Both RS experiments began with approximately the same number of clasts in contact with the bed, but the number of striations created during shear ($n_{\rm stria}$) varied between the two experiments (Table 1). Many clasts stopped abrading the bed before ice-ring rotation ceased in both experiments, although average striation length in experiment RS1 was a smaller fraction of the total displacement than in RS2. For DS experiments, indenting clasts commonly ploughed for the full displacement (\sim 1 cm).

Boundary conditions implemented in these experiments are purposefully diverse (Table 1), yet when normalized by bed area, measured shear force (F_s) scales linearly with abraded volume (V) for the same clast-bed combinations $(\sim 0.35 \text{ and } \sim 1.53 \text{ kN/}\mu\text{m})$ —implying a simple intrinsic relationship between the two parameters (Fig. 2). Contextualizing this with Equation 3 using parameters in Table 1 (assuming C is best represented by $n_{\text{stria}}/a_{\text{bed}}$), A increases linearly with $C_{\tau_r}u_s$ with erodibility constants for the limestone/granite (K_{ls}) and marble/granite (K_m) of $\sim 1.6 \times 10^{-10} \pm 1.7 \times 10^{-11} \text{ Pa}^{-1}$ and ${\sim}5.8 \times 10^{-12} \pm 7.4 \times 10^{-13} \ Pa^{-1},$ respectively. Notably, these values are $>10 \times$ smaller than prior estimates (Ugelvig and Egholm, 2018)

Given that ice slid over smooth plane beds in our experiments, work done during slip, W_b , relates primarily to clast-bed interactions. In other words, viscous deformation of the ice due to bed irregularities was minimized. We calculate W_b by subtracting background drag



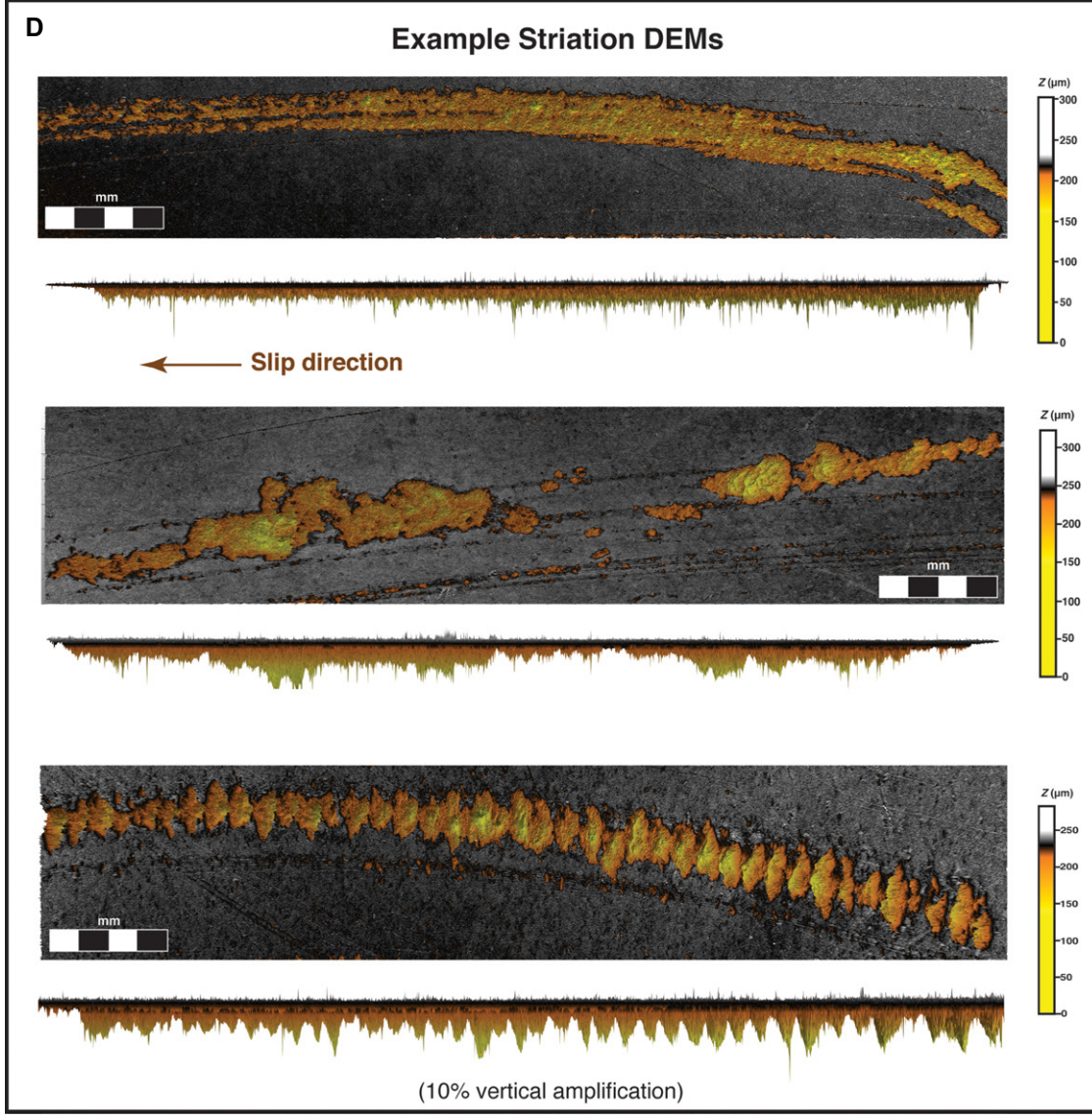


Figure 1. (A) Ring shear (RS) sample chamber with bed and clasts (no ice). (B) Ice ring with entrained clasts. (C) Striations left on the marble bed. (D) Three example striation digital elevation models (DEMs) in plan view and cross section. Color bars convey range of vertical position, z, for each respective DEM.

measured for each apparatus to obtain F_s and then numerically integrating F_s with respect to displacement using the trapezoidal rule. Figure 3 presents these data as work instead of power to facilitate comparison between the RS and DS experiments, which were run at different slip speeds. We find abrasion energy, E_a , (Equations 4–6) increases linearly with W_b for both bed types (Fig. 3), with approximately $\sim 0.14\%$ –

1.6% of $W_{\rm b}$ partitioned into abrasion. Although the estimated uncertainty is large relative to $E_{\rm a}$ for some data, the range represents ${\sim}1\%$ of $W_{\rm b}$ and therefore does not meaningfully impact our interpretation.

DISCUSSION AND CONCLUSIONS

Process-based models that incorporate the fundamental physics of abrasion offer the most

comprehensive look into its rates and dependencies (Melanson et al., 2013). This level of complexity, however, is not feasible for many applications, nor are the physics settled. Implementing a simplified abrasion rule that reduces the problem to one or two unknowns is therefore desirable. Typically, these parameterizations assume \dot{A} scales linearly or nonlinearly with u_s (Herman et al., 2021, references therein)

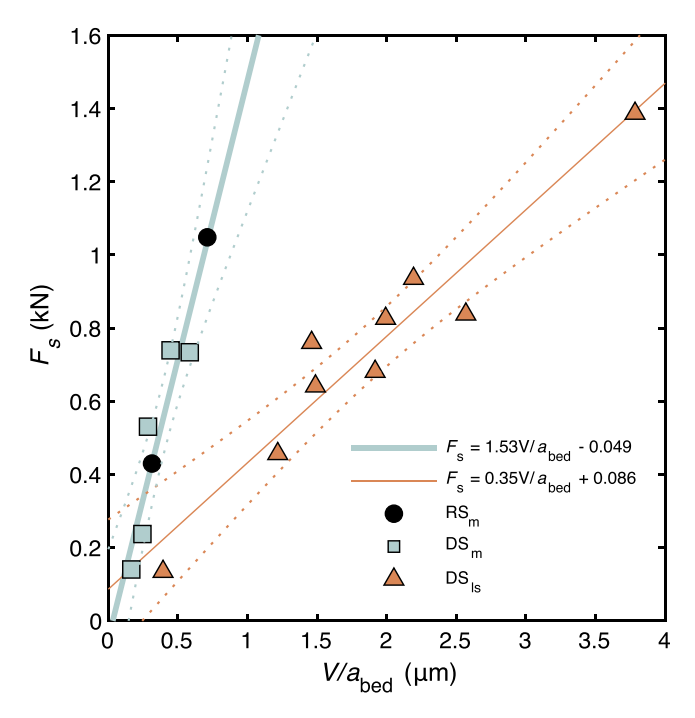


Figure 2. Abraded volume (V) normalized by the area of the bed (abed) scales linearly with mean shear force (F_s) for both ring shear (RS) and direct shear (DS) experiments and both clast-bed types (m—marble bed: –limestone bed). Solid lines are ordinary leastsquares fits, and dashed lines represent 95% confidence intervals. Standard error of the mean for F_s is smaller than the marker height.

but cannot capture the interdependence of τ_b and u_s . By including τ_b , Hallet's (2011) basal power abrasion law aimed to increase complexity while limiting unknown parameters to a single prefactor. Our results show his assumption that rock frictional energy scales with bedrock abrasion is correct for a plane bed and that an erodibility constant on the order of 10^{-12} to 10^{-10} Pa⁻¹) is a reasonable choice depending on lithology. Given the large hardness contrast between the soft limestone and the angular granite clasts in our experiments, our estimate for $K_{\rm ls}$ serves as a reasonable upper bound.

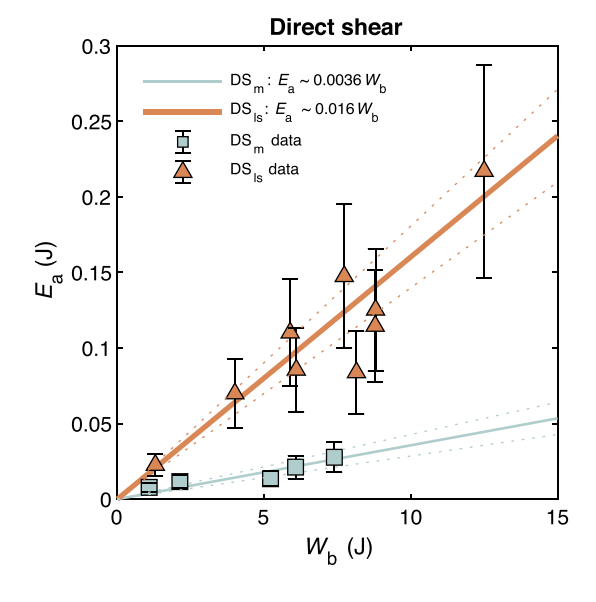
Although A scales linearly with basal power, drag in our experiments occurred solely from clast-bed interactions (i.e., $\tau_b \approx \tau_r$). Glacier beds, however, have roughness that obstructs ice

flow over a wide range of length scales (Anderson, 2014; Woodard et al., 2021). For till-free regions of the bed, resistance to motion is the summed contribution of drag related to viscous deformation and regelation of ice around bed obstacles, $\tau_{ice.}$ and subglacial rock friction (i.e., $\tau_b = \tau_{ice} + \tau_r$). Few constraints exist regarding the relative influence of these two mechanisms, but it depends on bed geometry, slip speed, effective stress, and controls on the contact force. Model results by Iverson et al. (2019) showed rock friction does not substantially alter the form of the sliding law for a sinusoidal bed but does increase τ_b . This increase is not strictly linear due to the interplay between cavity geometry and associated controls on F_n Data presented in Iverson et al.'s figures 7-9 imply $\tau_r u_s = \zeta(\tau_b u_s)^\beta$, where $\zeta \approx 0.0003$ –0.2 and $\beta \approx 1.1$ –1.6. β decreases with increasing clast size and increases with increasing bed roughness, and ζ responds inversely. Iverson et al. (2019) calculated F_n using Hallet's (1979) derivation, which subsequent experimental work by Thompson et al. (2020) showed is partially incorrect. This argues further work is needed to constrain the contribution of $\tau_r u_s$ to $\tau_b u_s$ for rough beds. However, as a first approximation for regions with undulating topography, Equation 3 could be modified to

$$\dot{A} = KC\zeta(\tau_{\rm b}u_{\rm s})^{\beta},\tag{7}$$

where ζ and β are likely on the lower and upper end, respectively, of the range implied by the model results in Iverson et al. (2019).

The linearity we observe between V/a_{bed} and F_s (Fig. 2) signals a possible method for constraining the proportionality between $\tau_r u_s$ and $\tau_b u_s$ empirically using field data. Abraded volume for hard-bedded glaciers may be extrapolated from suspended sediment yields in select cases if subglacial sediment storage is negligible on annual time scales. Knowing the relationship between V/a_{bed} and F_s , the area of the catchment, and annual volume of suspended sediment, one can infer integrated τ_r induced by abrading clasts. This would represent a minimum because it does not account for the frictional resistance of non-abrading clasts in contact with the bed, but it could be compared to derived values of $\tau_{\rm b}$. A source of uncertainty is the percentage of suspended fines produced through comminution of the abraders versus abrasion when debris abrades beds of the same lithology. It also assumes suspended sediment is entirely sourced from abrasion and comminution of quarried clasts in the fluvial system is negligible (Loso et al., 2004). Nonetheless, such a study could provide insight into the general magnitude of



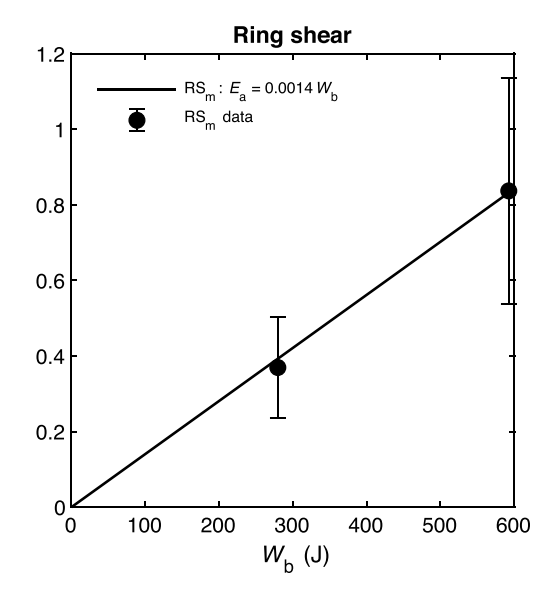


Figure 3. Energy dissipated through abrasion, E_a, increases linearly with work done during basal slip, W_b , in direct shear (DS) (left) and ring shear (RS) (right) experiments for both clast-bed types (m-marble bed; Is-limestone bed). Solid lines show weighted-least squares fit, and dotted lines show corresponding 95% confidence interval. Error bars denote median absolute deviation for 20,000 Monte Carlo Markov chain estimates of E_a .

clast-bed friction and the discrepancy between high τ_r recorded in situ (Cohen et al. 2005) and the generally low friction observed in ring-shear experiments (Thompson et al., 2020; Fig. S3).

Lastly and importantly, we find the percentage of W_h dissipated through abrasion in our experiments was $>10 \times$ lower than Metcalf's (1979) estimate at Nisqually Glacier (Washington State, USA). The root of this discrepancy is not clear, though we note most of our variables were measured directly whereas many aspects of his calculation had large uncertainties. Nevertheless, our value for limestone aligns with estimates for faults where the energy dissipated through crushing and gouging rock is \sim 1% of total work done during slip (Fulton and Rathbun, 2011). The remainder of W_b in our experiments was partitioned to other dissipative or radiative processes such as frictional heat generation or elastic radiated energy. Given this miniscule expenditure, it is not necessary to consider abrasion in parameterizations of glacial slip in ice-sheet models. However, this inefficient conversion of ice power to abrasion in no way diminishes its importance in sculpting glacial landscapes on geologic time scales.

ACKNOWLEDGMENTS

We thank R.S. Anderson, L.M. Simpkins, and an anonymous reviewer for their insightful reviews; S.E. Dodge for the grain-size analysis; H. Sone and M. Trzeciak for their expertise with the CCNBD and UCT experiments; and N. Lord and P. Sobol for designing the ring shear device and data collection software. This work is supported by U.S. National Science Foundation grant 2017185.

REFERENCES CITED

- Alley, R.B., Cuffey, K.M., and Zoet, L.K., 2019, Glacial erosion: Status and outlook: Annals of Glaciology, v. 60, p. 1–13, https://doi.org/10.1017/aog.2019.38.
- Anderson, R.S., 2014, Evolution of lumpy glacial landscapes: Geology, v. 42, p. 679–682, https://doi.org/10.1130/G35537.1.
- Andrews, J.T., 1972, Glacier power, mass balances, velocities and erosion potential: Zeitschrift für Geomorphologie, v. 13, p. 1–17.
- Benn, D.I., and Evans, D.J.A., 2010, Erosional Processes, Forms, and Landscape, *in* Benn, D.I., and

- Evans, D.J.A., eds., Glaciers and Glaciation: London, Routledge, p. 261–332, https://doi.org/10.4324/9780203785010.
- Cohen, D., Iverson, N.R., Hooyer, T.S., Fischer, U.H., Jackson, M., and Moore, P.L., 2005, Debris-bed friction of hard-bedded glaciers: Journal of Geophysical Research: Earth Surface, v. 110, F02007, https://doi.org/10.1029/2004JF000228.
- Drewry, D.J., 1986, Glacial Geologic Processes: London, Edward Arnold, 276 p.
- Fulton, P.M., and Rathbun, A.P., 2011, Experimental constraints on energy partitioning during stickslip and stable sliding within analog fault gouge: Earth and Planetary Science Letters, v. 308, p. 185–192, https://doi.org/10.1016/j.epsl.2011 .05.051.
- Hallet, B., 1979, A theoretical model of glacial abrasion: Journal of Glaciology, v. 23, p. 39–50, https://doi.org/10.3189/S0022143000029725.
- Hallet, B., 2011, Glacial erosion assessment: Toronto, Canada, Nuclear Waste Management Organization Report NWMO DGR-TR-2011-18, 55 p.
- Hallet, B., Hunter, L., and Bogen, J., 1996, Rates of erosion and sediment evacuation by glaciers: A review of field data and their implications: Global and Planetary Change, v. 12, p. 213–235, https://doi.org/10.1016/0921-8181(95)00021-6.
- Hansen, D.D., and Zoet, L.K., 2019, Experimental constraints on subglacial rock friction: Annals of Glaciology, v. 60, p. 37–48, https://doi.org/10 .1017/aog.2019.47.
- Hansen, D.D., and Zoet, L.K., 2022, Characterizing sediment flux of deforming glacier beds: Journal of Geophysical Research: Earth Surface, v. 127, e2021JF006544, https://doi.org/10.1029/2021JF006544.
- Herman, F., De Doncker, F., Delaney, I., Prasicek, G., and Kopes, M., 2021, The impact of glaciers on mountain erosion: Nature Reviews Earth & Environment, v. 2, p. 422–435, https://doi.org/10.1038/s43017-021-00165-9.
- Iverson, N.R., 1991, Morphology of glacial striae: Implications for abrasion of glacier beds and fault surfaces: Geological Society of America Bulletin, v. 103, p. 1308–1316, https://doi.org/10.1130/0016-7606(1991)103<1308:MOGSIF>2.3.CO:2.
- Iverson, N.R., Helanow, C., and Zoet, L.K., 2019, Debris-bed friction during glacier sliding with ice-bed separation: Annals of Glaciology, v. 60, p. 30–36, https://doi.org/10.1017/aog.2019.46.
- Loso, M.G., Anderson, R.S., and Anderson, S.P., 2004, Post–Little Ice Age record of coarse and fine clastic sedimentation in an Alaskan proglacial lake: Geology, v. 32, p. 1065–1068, https://doi.org/10.1130/G20839.1.

- Melanson, A., Bell, T., and Tarasov, L., 2013, Numerical modelling of subglacial erosion and sediment transport and its application to the North American ice sheets over the Last Glacial cycle: Quaternary Science Reviews, v. 68, p. 154–174, https://doi.org/10.1016/j.quascirev.2013.02.017.
- Metcalf, R.C., 1979, Energy dissipation during subglacial abrasion at Nisqually Glacier, Washington, USA: Journal of Glaciology, v. 23, p. 233–246, https://doi.org/10.3189/S0022143000029865.
- Molnar, P., and England, P., 1990, Late Cenozoic uplift of mountain ranges and global climate change: Chicken or egg?: Nature, v. 346, p. 29–34, https:// doi.org/10.1038/346029a0.
- Nye, J.F., 1957, The distribution of stress and velocity in glaciers and ice-sheets: Proceedings of the Royal Society: Series A, Mathematical and Physical Sciences, v. 239, p. 113–133, https://doi.org/10.1098/rspa.1957.0026.
- Nye, J.F., 1976, Water flow in glaciers: Jökulhlaups, tunnels and veins: Journal of Glaciology, v. 17, p. 181–207, https://doi.org/10.1017 /S002214300001354X.
- Thompson, A.C., Iverson, N.R., and Zoet, L.K., 2020, Controls on subglacial rock friction: Experiments with debris in temperate ice: Journal of Geophysical Research: Earth Surface, v. 125, e2020JF005718, https://doi.org/10.1029/2020JF005718.
- Ugelvig, S.V., and Egholm, D.L., 2018, The influence of basal-ice debris on patterns and rates of glacial erosion: Earth and Planetary Science Letters, v. 490, p. 110–121, https://doi.org/10.1016/j.epsl.2018.03.022.
- Weertman, J., 1957, On the sliding of glaciers: Journal of Glaciology, v. 3, p. 33–38, https://doi.org/10.1017/S0022143000024709.
- Whipple, K.X, and Tucker, G.E., 1999, Dynamics of the stream-power river incision model: Implications for height limits of mountain ranges, landscape response timescales, and research needs: Journal of Geophysical Research, v. 104, p. 17,661–17,674, https://doi.org/10.1029/1999JB900120.
- Woodard, J.B., Zoet, L.K., Iverson, N.R., and Helanow, C., 2021, Variations in hard-bedded topography beneath glaciers: Journal of Geophysical Research: Earth Surface, v. 126, e2021JF006326, https://doi.org/10.1029/2021JF006326.
- Zoet, L.K., Carpenter, B., Scuderi, M., Alley, R.B., Anandakrishnan, S., Marone, C., and Jackson, M., 2013, The effects of entrained debris on the basal sliding stability of a glacier: Journal of Geophysical Research: Earth Surface, v. 118, p. 656–666, https://doi.org/10.1002/jgrf.20052.

Printed in USA